ELSEVIER

Journal of Alloys and Compounds 452 (2008) 16–22

Journal of ALLOYS AND COMPOUNDS

www.elsevier.com/locate/jallcom

Surface morphology of scale on FeCrAl (Pd, Pt, Y) alloys

T. Amano [a,*], Y. Takezawa [a], A. Shiino [a], T. Shishido [b]

[a] *Department of Materials Science and Engineering, Shonan Institute of Technology, Fujisawa 251-8511, Japan*
[b] *Institute for Materials Research, Tohoku University, Sendai 980-8577, Japan*

Received 18 September 2006; received in revised form 1 January 2007; accepted 6 January 2007
Available online 20 February 2007

Abstract

The high temperature oxidation behavior of Fe–20Cr–4Al, floating zone refined (FZ) Fe–20Cr–4Al, Fe–20Cr–4Al–0.5Pd, Fe–20Cr–4Al–0.5Pt and Fe–20Cr–4Al–(0.01, 0.02, 0.05, 0.1, 0.2, 0.5)Y alloys was studied in oxygen for 0.6–18 ks at 1273–1673 K by mass gain measurements, X-ray diffraction and scanning electron microscopy. The mass gains of FeCrAl, FZ FeCrAl, FeCrAlPd and FeCrAlPt alloys showed almost the same values. Those of FeCrAl–(0.01, 0.02, 0.05, 0.1, 0.2, 0.5)Y alloys decreased with increasing yttrium of up to 0.1% followed by an increase with the yttrium content after oxidation for 18 ks at 1473 K. Needle-like oxide particles were partially observed on FeCrAl alloy after oxidation for 7.2 ks at 1273 K. These oxide particles decreased in size with increasing oxidation time of more than 7.2 ks at 1473 K, and then disappeared after oxidation for 7.2 ks at 1573 K. It is suggested that a new oxide develops at the oxygen/scale interface. The scale surface of FeCrAl alloy showed a wavy morphology after oxidation for 7.2 ks at 1273 K which then changed to planar morphology after an oxidation time of more than 7.2 ks at 1573 K. On the other hand, the scale surfaces of other alloys were planar after all oxidation conditions in this study. The scale surfaces of FeCrAl, FZ FeCrAl, FeCrAlPd and FeCrAlPt alloys were rough, however, those of FeCrAl–(0.1, 0.2, 0.5)Y alloys were smooth. The oxide scales formed on FeCrAl–(0.1, 0.2, 0.5)Y alloys were found to be α-Al_2O_3 with small amounts of $Y_3Al_5O_{12}$, and those of the other alloys were only α-Al_2O_3.

Keywords: Oxide adherence; Alumina scale; Palladium; Platinum; Yttrium

1. Introduction

An oxide scale of α-Al_2O_3 forms on the alloys when alumina-forming heat-resistant alloys are exposed to high temperatures of more than 1273 K in oxidizing atmospheres. The α-Al_2O_3 scale often spalls during cooling after oxidation. Various hypotheses have been offered to explain the spalling of the oxide scale, and interest has been recently focused on the segregation of sulfur at the oxide/alloy interface [1–12]. On the other hand, to improve the oxide adherence, many studies have been conducted with regard to the effect of small additions of reactive elements such as rare earths, zirconium, and hafnium [13–23]. Recently, high temperature oxidation studies of heat-resistant alloys containing controlled levels of both sulfur and reactive elements have been conducted, however, the oxidation behavior of such alloys is complicated [2–4,7,11,17–23]. On the other hand, the effects of small noble metal (Pd, Rh, Pt) additions on the oxidation behavior of the Al_2O_3-forming heat-resistant alloys have been also studied [24–27].

In the present study, the surface morphology of scale on FeCrAl (standard, FZ, Pd, Pt, Y) alloys was studied in oxygen at 1273–1673 K for oxidation times of 0.6–18 ks, in order to clarify the relationship between oxide adherence and noble metal or yttrium addition.

2. Experimental

Buttons weighing 50 g were prepared by arc-melting in a water-cooled hearth in an argon atmosphere. The base composition of the alloys was nominally FeCrAl with 4 ppm sulfur, to which palladium or platinum of 0.5% and yttrium of 0.01, 0.02, 0.05, 0.1, 0.2 or 0.5% were added. The floating zone refined (FZ) FeCrAl alloy was made by floating zone melting of the alloy with 4 ppm S. The compositions of the alloys are given in Table 1. The buttons were hot- and cold-rolled to a sheet of 0.5 mm thickness. The specimens were then cut to dimensions of about 0.5 mm × 10 mm × 20 mm, and were polished through 1500 grit SiC paper. The specimens (5 mm × 5 mm × 0.5 mm) used for the investigation of oxide morphological change were mirror-polished with diamond paste (3 μm) after initial polishing. Each specimen was cleaned ultrasonically in alcohol before being tested. Oxidation tests were conducted in flowing oxygen (100 cm^3/min) for 18 ks at 1473 K. The mass gain was measured after oxidation,

* Corresponding author. Tel.: +81 466 30 0225; fax: +81 466 30 0225.
E-mail address: amano@mate.shonan-it.ac.jp (T. Amano).

0925-8388/$ – see front matter © 2007 Elsevier B.V. All rights reserved.
doi:10.1016/j.jallcom.2007.01.170

Table 1
Chemical compositions of alloys used for the investigations (mass%)

Alloy	Fe	Cr	Al	S	Pd	Pt	Y
Fe–20Cr–4Al (standard)	Balance	20	4	0.0004	–	–	–
FZ Fe–20Cr–4Al[a]	Balance	20	4	<0.0001	–	–	–
Fe–20Cr–4Al–0.5Pd	Balance	20	4	0.0001	0.498	–	–
Fe–20Cr–4Al–0.5Pt	Balance	20	4	0.0001	–	0.499	–
Fe–20Cr–4Al–0.01Y	Balance	20	4	0.0001	–	–	0.0001
Fe–20Cr–4Al–0.02Y	Balance	20	4	0.0001	–	–	0.0002
Fe–20Cr–4Al–0.05Y	Balance	20	4	0.0001	–	–	0.0023
Fe–20Cr–4Al–0.1Y	Balance	20	4	0.0001	–	–	0.0382
Fe–20Cr–4Al–0.2Y	Balance	20	4	0.0001	–	–	0.0980
Fe–20Cr–4Al–0.5Y	Balance	20	4	0.0001	–	–	0.3449

[a] FZ Fe–20Cr4Al is purified by floating zone melting in hydrogen.

and the appearance of samples was also observed. The oxide formed on the alloys was identified by X-ray diffraction (XRD). The oxide morphology was observed by scanning electron microscopy (SEM). Another experiment was then carried out in order to clarify the oxide morphology by the various times and temperatures of oxidation. The oxide morphology was observed by SEM after oxidation, and then the alloys were again exposed to oxygen. This process was continued. The alloys were exposed to oxygen for 7.2 and 18 ks at 1273 K, 1.8 and 18 ks at 1373 K, 0.6, 7.2 and 18 ks at 1473 K, 1.8 and 7.2 ks at 1573 K and 18 ks at 1673 K.

3. Results

3.1. Mass gain

The mass gain of the FeCrAl (standard, FZ, 0.5Pd, 0.5Pt) alloys exposed to oxygen for 18 ks at 1473 K. Mass gains of all the alloys were between 5.0 and 5.2×10^{-3} kg m^{-2}. As is mentioned in the later part, spalling of the scale on the standard alloy occurred from the entire surface. The mass of the spalled oxide is added in the mass gain of the alloy. Fig. 1 shows the mass gain of the FeCrAlY alloys exposed to oxygen for 18 ks at 1473 K. Mass gain of the alloys decreased up to 0.1% yttrium, and then increased with increasing yttrium content.

3.2. Surface appearance and X-ray diffraction

Fig. 2 shows the surface appearance of the FeCrAl alloys exposed to oxygen for 18 ks at 1473 K. The surface of all the alloys, except the standard alloy, was covered with oxide scale. Oxide scale on the standard alloy spalled from the entire surface, and spalling of the oxide scale on the FZ, 0.5Pd and 0.5Pt was scarcely found. The oxide scale on the 0.01Y alloy slightly spalled, and those on the 0.02Y and 0.05Y alloys faintly spalled, however, no spalling of those on the 0.1Y, 0.2Y and 0.5Y alloys was found. Scale color of the 0.5Pd was brown, and those of the 0.1Y, 0.2Y and 0.5Y alloys were glossy gray. On the other hand, those of the other alloys were gray.

Table 2 shows oxides determined by X-ray diffraction of the FeCrAl alloys exposed to oxygen for 18 ks at 1473 K. Oxide scale on all the alloys was mainly found as α-Al_2O_3. $Y_3Al_5O_{12}$ was recognized in 0.2Y and 0.5Y alloys, and its peak intensity increased with increasing yttrium content.

3.3. Scanning electron microscopy

Fig. 3 shows typical surface views of the FeCrAl alloys exposed to oxygen for 18 ks at 1473 K. The oxide surface on the standard, FZ, 0.5Pd, 0.5Pt, 0.01Y, 0.02Y and 0.05Y alloys

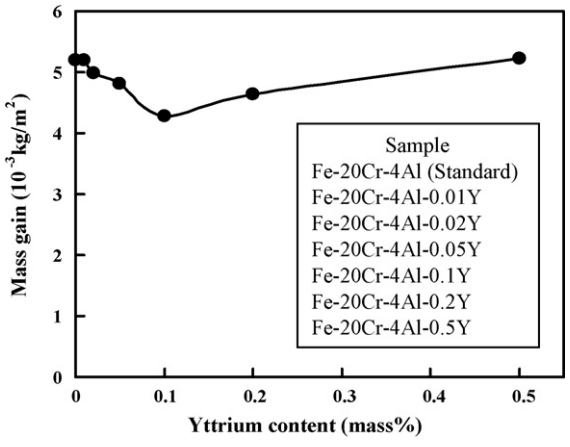

Fig. 1. Mass gain of FeCrAl (0.01–0.5Y) alloys exposed to oxygen for 18 ks at 1473 K.

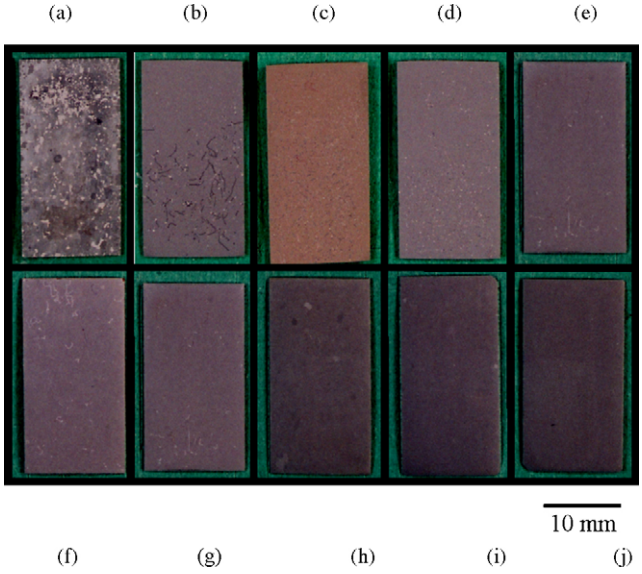

Fig. 2. Surface appearance of FeCrAl alloys exposed to oxygen for 18 ks at 1473 K. (a) Standard; (b) FZ; (c) 0.5Pd; (d) 0.5Pt; (e) 0.01Y; (f) 0.02Y; (g) 0.05Y; (h) 0.1Y; (i) 0.2Y; (j) 0.5Y.

Table 2
Oxides determined by X-ray diffraction of FeCrAl alloys exposed to oxygen for 18 ks at 1473 K (the peak intensities of the oxide are indicated in parentheses)

Standard	α-Al_2O_3 (w)
FZ	α-Al_2O_3 (s)
0.5Pd	α-Al_2O_3 (s)
0.5Pt	α-Al_2O_3 (s)
0.01Y	α-Al_2O_3 (s)
0.05Y	α-Al_2O_3 (s)
0.1Y	α-Al_2O_3 (s)
0.2Y	α-Al_2O_3 (s) $Y_3Al_5O_{12}$ (vw)
0.5Y	α-Al_2O_3 (s) $Y_3Al_5O_{12}$ (w)

s: strong, w: weak, wv: very weak.

was rough, and that on the 0.1Y, 0.2Y and 0.5Y alloys was smooth. The oxide surface on the standard alloy showed a wavy morphology, and that on the Y-added alloys changed to planar with increasing yttrium content. The surfaces of the standard, FZ, 0.5Pd, 0.5Pt, 0.01Y, 0.02Y and 0.05Y alloys showed reticular microstructure, and many cavities were found in the scale surface. Cavities in the scale surface of the standard, FZ, 0.5Pd, 0.5Pt, 0.01Y, 0.02Y, 0.05Y, 0.1Y and 0.2Y alloys were 1.0, 1.0, 1.0, 1.0, 0.5, 0.5, 0.4, 0.13 and 0.07 μm in size from SEM observation by a factor of 1000 or 3000, however, cavities in the scale surface of 0.5Y alloy were not detected. The granular oxide $Y_3Al_5O_{12}$ particles (as is mentioned in the later part) on the scale of 0.1Y, 0.2Y and 0.5Y alloys were about 1, 2 and 4 μm in size, respectively, and these oxide particles increased with increasing yttrium content. Since amounts of $Y_3Al_5O_{12}$ particles were a trace as shown in Fig. 3(h), the $Y_3Al_5O_{12}$ phase was not found by X-ray diffraction (Table 2).

3.4. Scanning electron microscopy (change with time and temperature of oxidation)

In order to clarify oxidation behavior of heat-resistant alloys, the growth process of the oxide scale was studied by change with time and temperature of oxidation. As is mentioned in the later part, main oxide scale α-Al_2O_3 is formed on the alloys when alumina-forming heat-resistant alloys are exposed to oxygen at 1273 K, however, the formation of transient alumina phase such as needle-like θ-Al_2O_3 is partially found on the oxide scale. The oxidation experiment was carried out for 7.2 and 18 ks at

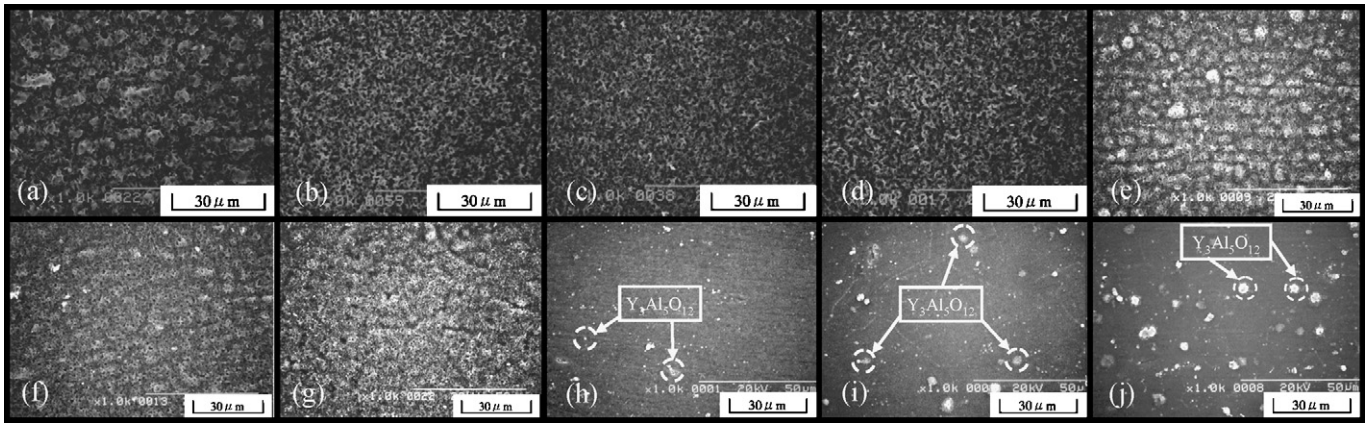

Fig. 3. SEM micrographs of the oxide scale on FeCrAl alloys exposed to oxygen for 18 ks at 1473 K. (a) Standard; (b) FZ; (c) 0.5Pd; (d) 0.5Pt; (e) 0.01Y; (f) 0.02Y; (g) 0.05Y; (h) 0.1Y; (i) 0.2Y; (j) 0.5Y.

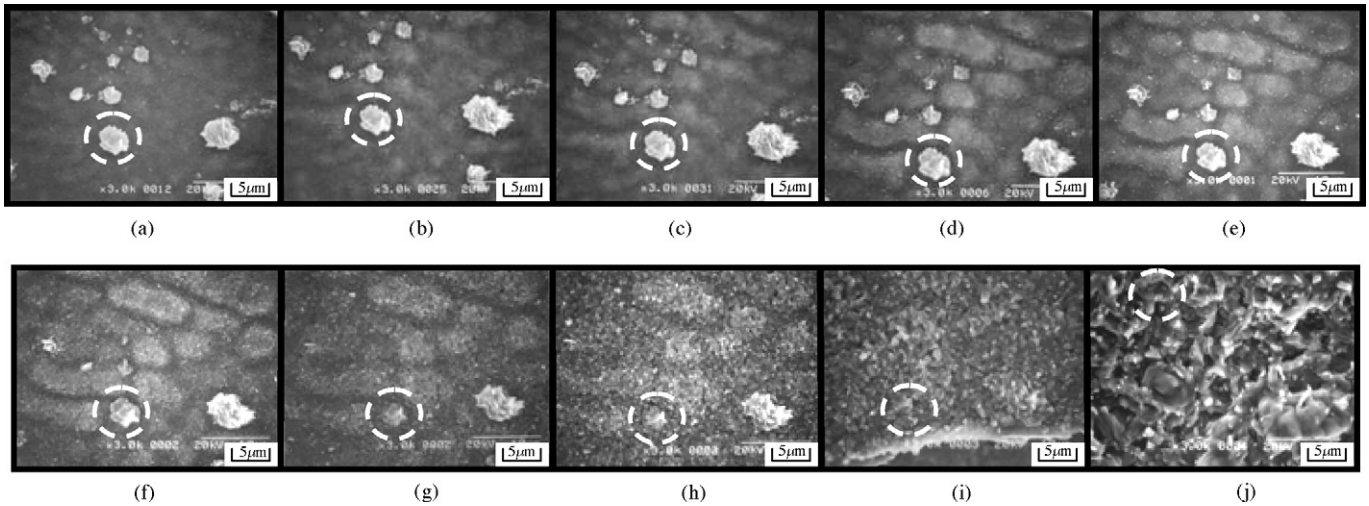

Fig. 4. SEM micrographs of the oxide scale on FeCrAl (standard) alloy exposed to oxygen for 0.6 ~ 18 ks at 1273–1673 K. (a) 1273 K, 7.2 ks; (b) 1273K, 18 ks; (c) 1373 K, 1.8 ks; (d) 1373 K, 18 ks; (e) 1473 K, 0.6 ks; (f) 1473 K, 7.2 ks; (g) 1473 K, 18 ks; (h) 1573 K, 1.8 ks; (i) 1573 K, 7.2 ks; (j) 1673 K, 18 ks.

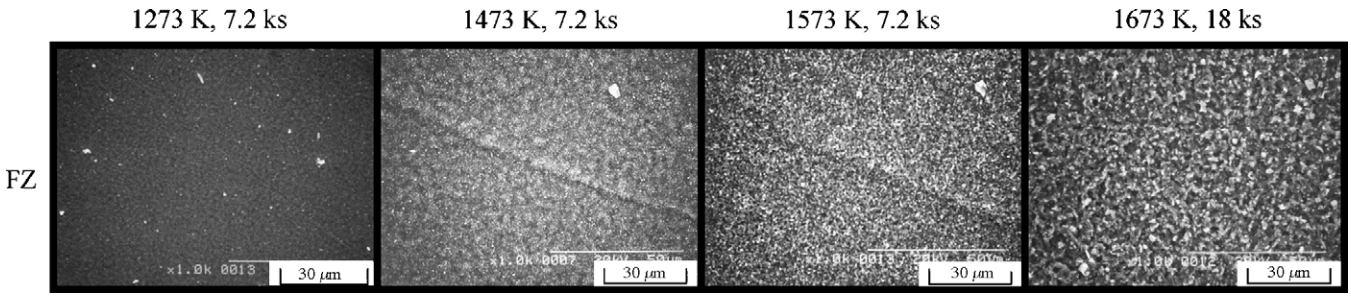

Fig. 5. SEM micrographs of the oxide scale on FeCrAl (FZ) alloys exposed to oxygen at 1273–1673 K.

1273 K, 1.8 and 18 ks at 1373 K, 0.6, 7.2 and 18 ks at 1473 K, 1.8 and 7.2 ks at 1573 K and 18 ks at 1673 K. Fig. 4 shows surface morphologies of the standard alloy exposed to oxygen at high temperatures. Needle-like oxide particles on the standard alloy were partially observed by SEM after oxidation at 1273 K for 7.2 ks (Fig. 4(a)). After that the same sample was again exposed to oxygen and the same place was observed in order to investigate the change of needle-like oxide morphology. These needle-like oxide particles are thought to be θ-Al_2O_3 as reported by Tolpygo and Clarke [28], and Hou et al. [29]. The experimental method was repeated. The diameter of needle-like oxide θ-Al_2O_3 particle was 4.1 μm (Fig. 4(a)) which was almost the same in size after oxidation at 1473 K for 7.2 ks (Fig. 4(f)). However, the particle size was 3.8 μm after oxidation at 1473 K for 18 ks (Fig. 4(g)). The particle after oxidation at 1573 K for 1.8 and 7.2 ks was 3.5 and 2.9 μm in size, respectively (Fig. 4h and i). The surrounding main oxide scale, α-Al_2O_3, of the oxide particle grew by outward transport of aluminum. Its longitudinal dimension approached that of needle-like oxide after oxidation at 1573 K for 7.2 ks (Fig. 4(i)). Scale surface (α-Al_2O_3) on the standard alloy (except θ-Al_2O_3) was planar after oxidation at 1273 K for 7.2 ks, and the scale surface changed to a wavy morphology after oxidation at 1373 K for 18 ks (Fig. 4(d)). After that the scale surface tended to planar with increasing time and temperature of oxidation and became definitely planar after oxidation at 1573 K for 7.2 ks (Fig. 4(i)). A reticular structure on the

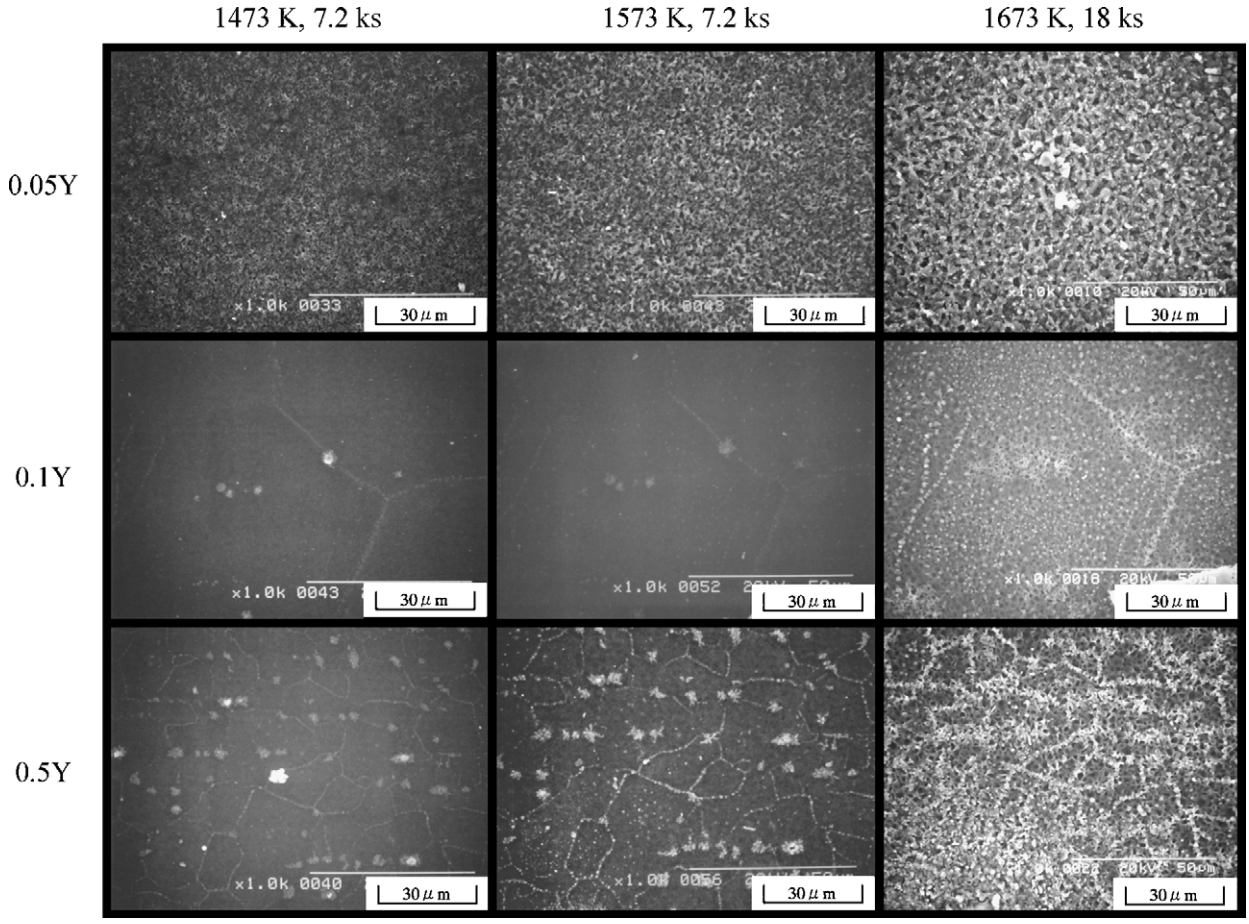

Fig. 6. SEM micrographs of the oxide scale on FeCrAl (0.05Y, 0.1Y, 0.5Y) alloys exposed to oxygen at 1473–1673 K.

alloy was found on the scale surface after oxidation at 1473 K for 7.2 ks. The formation of cavities was observed in the surface oxide, and the cavities increased in size with increasing time and temperature of oxidation. The size of the cavities was 0.3 and 0.5 μm after oxidation at 1473 K for 7.2 and 18 ks which increased to 0.6 and 1.0 μm after oxidation at 1573 K for 1.8 and 7.2 ks, respectively. After oxidation at 1673 K for 18 ks the size of cavities was 3 μm. Fig. 5 shows the scale surface of the FZ alloy after oxidation at 1273 K for 7.2 ks, 1473 K for 7.2 ks, 1573 K for 7.2 ks and 1673 K for 18 ks. The scale surface on the alloy was planar after independent of the oxidation conditions. A reticular structure on the alloy (except after oxidation at 1273 K for 7.2 ks) was observed at all oxidation conditions, and the cavities in the oxide surface increased with increasing oxidation temperature. The size of the cavities was 0.2, 1.0 and 2.0 μm after oxidation at 1473 K for 7.2 ks, 1573 K for 7.2 ks and 1673 K for 18 ks, respectively. The scale surface of the 0.5Pd and 0.5Pt alloys observed at the same oxidation conditions was almost the same as that of the FZ alloy. Fig. 6 shows the scale surface of the 0.05Y, 0.1Y and 0.5Y alloys after oxidation at 1473 K for 7.2 ks, 1573 K for 7.2 ks and 1673 K for 18 ks. The scale surface of all the alloys showed a planar morphology irrespective of the oxidation conditions. Reticular structures on the 0.05Y alloy were observed at all oxidation conditions. Those on the 0.1Y and 0.5Y alloy were found after oxidation at 1673 K for 18 ks. The size of the cavities on the 0.05Y alloy increased with increasing oxidation temperature. It was 0.5, 1.5 and 2.0 μm after oxidation at 1473 K for 7.2 ks, 1573 K for 7.2 ks and 1673 K for 18ks, respectively. The cavities on the 0.1Y and 0.5Y alloys were about 1.0 μm in size. $Y_3Al_5O_{12}$ particles on 0.1Y and 0.5Y alloys were observed at the grain boundaries and in the grains. The number of $Y_3Al_5O_{12}$ particles increased with increasing oxidation temperature and yttrium content. The size of $Y_3Al_5O_{12}$ particles on the 0.1Y and 0.5Y alloys were the same (about 1 μm). The grain size of the 0.1Y and 0.5Y alloys was 100 and 25 μm, respectively. Fig. 7 shows the same place on the oxide surface of the standard alloy after oxidation (a) at 1573 K for 7.2 ks and (b) at 1673 K for 18 ks. The spalled area on the alloy (Fig. 7(a)) was covered with the oxide scale (Fig. 7(b)), and the oxide/alloy interface was not found after oxidation at 1673 K for 18 ks.

4. Discussion

The mass gains of the standard, FZ, 0.5Pd and 0.5Pt alloys were similar in value. Those of the alloys with yttrium decreased up to 0.1% yttrium and then increased with increasing yttrium content after oxidation at 1473 K for 18 ks in oxygen. This result suggested that the mass gains of the FeCrAl alloys are scarcely affected by small amounts of sulfur, Pd and Pt, and that the formation of a dense Al_2O_3 scale due to the addition of up to 1% yttrium decreases the diffusion rate of oxygen and/or aluminum ions. On the other hand, the addition of yttrium also increases the mass gain, since the free energy of formation of Y_2O_3 is a little more negative than that of Al_2O_3 [30]. In this study, most of the yttrium was present as a Y–Fe intermetallic compound precipitated at the grain boundaries and was probably active. Therefore, Y_2O_3 particles were selectively formed at the grain boundaries and acted as nuclei and short circuit diffusion paths of oxygen for the formation of Al_2O_3. Consequently Al_2O_3 grew surrounding the Y_2O_3 particles followed by the formation of $Y_3Al_5O_{12}$ particles due to the reaction of Y_2O_3 with Al_2O_3. Therefore, the additions of yttrium decreases the mass gain because of the formation of dense oxide and reads to increase because of the rapid oxidation rate of yttrium and the subsequent rapid diffusion rate of oxygen and yttrium through the $Y_3Al_5O_{12}$ particles. Total mass gain is obtained as a result of both. Granular oxide particles of $Y_3Al_5O_{12}$ were observed at the scale surface of 0.1Y, 0.2Y and 0.5Y alloys. The $Y_3Al_5O_{12}$ particles increased in number as the yttrium content increased [11,13,16,19,31].

Table 3 shows the oxide feature of the FeCrAl alloys exposed to oxygen at 1473 K for 18 ks. As mentioned above, oxide scale on the standard alloy spalled from the entire surface. Four parts per million sulfur was contained in the standard alloy as impurity. Forest and Davidson [32] suggested that the oxide/alloy interface in the FeCrAl alloys containing less than 2 ppm of sulfur resisted growth stresses in the oxide. The oxide remained adherent and the alloys containing 4 ppm of sulfur caused considerable spalling. The present authors [12] also suggested that the FeCrAl alloys containing 1 and 3 ppm of sulfur shows good oxide adherence, and all of the alloys containing 4, 7, 35 and

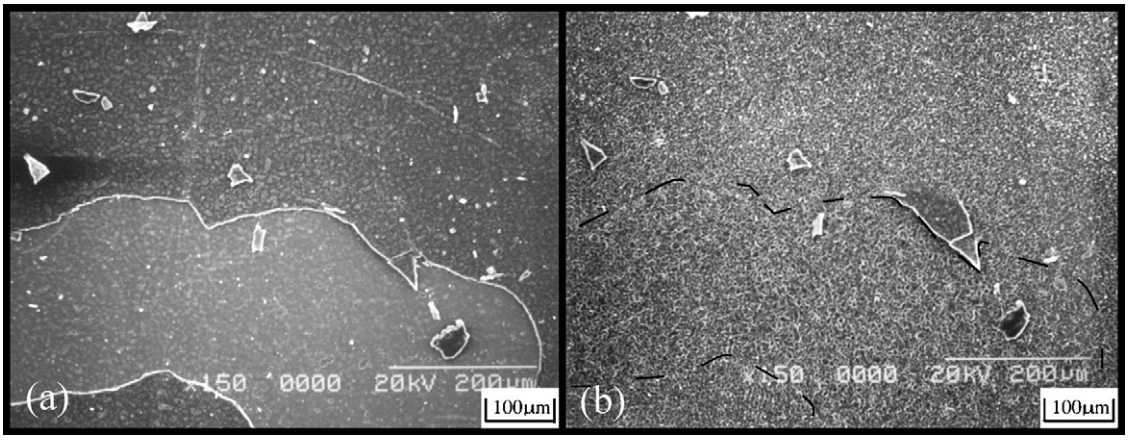

Fig. 7. SEM micrographs of the oxide scale on FeCrAl (standard) alloy exposed to oxygen (a) for 7.2 ks at 1573 K and then (b) for 18 ks at 1673 K.

Table 3
Summary of the scale feature on FeCrAl alloys exposed to oxygen for 18 ks at 1473 K

Alloy	Scale feature
Fe–20Cr–4Al (standard)	Entirely spalled, rough, wavy, facial cavity (1 μm), gray
FZ Fe–20Cr–4Al	Faintly spalled, rough, facial cavity (1 μm), gray
Fe-20Cr–4Al–0.5Pd	Faintly spalled, rough, facial cavity (1 μm), brown
Fe–20Cr–4Al–0.5Pt	Faintly spalled, rough, facial cavity (1 μm), gray
Fe–20Cr–4Al–0.01Y	Slightly spalled, rough, wavy, facial cavity (0.5 μm), gray
Fe–20Cr–4Al–0.02Y	Faintly spalled, rough, slightly wavy, facial cavity (0.5 μm), gray
Fe–20Cr–4Al–0.05Y	Faintry spalled, rough, slightly wavy, facial cavity (0.4 μm), gray
Fe–20Cr–4Al–0.1Y	No spalled, smooth, facial cavity (0.13 μm, glossy gray, fine $Y_3Al_5O_{12}$ particle (1 μm g.b.)
Fe–20Cr–4Al–0.2Y	No spalled, smooth, facial cavity (0.07 μm, glossy gray, fine $Y_3Al_5O_{12}$ particle (3 μm g.b.)
Fe–20Cr–4Al–0.5Y	No spalled, smooth, glossy gray, fine $Y_3Al_5O_{12}$ particle (5 μm g.b., g.)

No < faintly < slightly < entirely. g.b., gain boundary and g., grain.

53 ppm of sulfur caused considerable spalling after oxidation at 1473 K for 18 ks in oxygen. Spalling of the oxide scale might be caused by the segregation of sulfur at the oxide/alloy interface [1–12]. The wavy morphology on the scale surface was formed by the development of a new oxide in the scale and this leads to the spalling of oxide scale. On the other hand, the spalling of the oxide scale on the other alloys was scarcely observed. The good oxide adherence may be caused by these low sulfur contents less than 3 ppm [3,5,9–12,32]. The cavities in the scale surface of all the alloys, except the 0.5Y alloy, were found after oxidation at 1473 K for 18 ks. Cavity formation may occur by grain growth of Al_2O_3 possibly by the outward diffusion of aluminum ions [33]. The size of the cavities decreased with increasing yttrium content. This result suggested that yttrium additions decreased the outward diffusion of aluminum ion because of the formation of a dense oxide scale on the alloys.

A protective α-Al_2O_3 is formed during oxidation at temperatures around 1473 K [3,6,9–16,18,19,21,22,31–33]. At low temperatures, the scale may contain metastable (transient) aluminas, such as γ-Al_2O_3 and θ-Al_2O_3 [28,29,31]. The transient aluminas are often described as platelet- or needle-like morphology [28,29] growing 1–2 orders of magnitude faster than α-Al_2O_3 [34] due to the growth dominated mainly by outward transport of aluminum [35]. In this study, the change of the needle-like oxide morphology was studied by varying time and temperature of oxidation. The oxide scale after oxidation at 1273 K for 7.2 ks was mainly α-Al_2O_3 with some amount of θ-Al_2O_3 oxide particles [28]. The θ-Al_2O_3 particles transformed to α-Al_2O_3 with increasing oxidation time and oxidation temperature [28,29,31]. Since this transformation was accompanied by a volume decrease of 12% voids were formed in the scale [28]. The void formation might also have been one of reason of oxide spallation. The size and morphology of the θ-Al_2O_3 particles was investigated during oxidation. One of θ-Al_2O_3 particles was about 4.1 μm in size after oxidation at 1273 K for 7.2 ks in oxygen and kept its the size after oxidation at 1473 K for 7.2 ks. However, after oxidation at 1473 K for 18 ks the size of the particle was 3.8 μm, and after oxidation at 1573 K for 1.8 and 7.2 ks was 3.5 and 2.9 μm. These results suggested that the size of this needle-like oxide particle decreased with increasing time and temperature of oxidation. On the other hand, the surrounding oxide of the needle-like oxide grows towards scale surface with increasing time and temperature of oxidation. The height of the oxide scale was the same as that of the needle-like oxide after oxidation at 1573 K for 7.2 ks. When the alloy substrate, which was the spalled area of oxide scale after oxidation at 1573 K for 7.2 ks, was again oxidized at 1673 K for 18 ks the area was covered with a planar oxide scale as shown in Fig. 7. These results suggested that the growth of the oxide scale occurs at the oxygen/scale interface by outward diffusion of aluminum. However, this result never refers to the scale growth at the scale/alloy interface [36].

5. Conclusions

The surface morphology of scales on the FeCrAl (standard: 4 ppm S), FeCrAl (FZ:<1 ppm S) purified by floating zone melting, FeCrAlPd, FeCrAlPt and FeCrAlY alloys was studied in oxygen after an exposure of 0.6–18 ks at 1273–1673 K.

After oxidation at 1473 K for 18 ks, the scale surface on the standard alloy showed a wavy morphology while that with yttrium addition changed to a smooth morphology which increased with the yttrium content. The scale surface on the 0.1Y, 0.2Y, 0.5Y, FZ, 0.5Pd and 0.5Pt alloys was planar. On the other hand, cavities were found on the scale surface of the standard, FZ, 0.5Pd, 0.5Pt, 0.01Y, 0.02Y, 0.05Y, 0.1Y and 0.2Y alloys. Their sizes were 1.0, 1.0, 1.0, 1.0, 0.5, 0.5, 0.4, 0.13 and 0.07 μm, respectively. No cavities on the alloy with 0.5Y were found.

From the changes with time and temperature of oxidation, needle-like oxide particles were partially found at scale surface of the standard alloy after oxidation at 1273 K for 7.2 ks. The size of the particles decreased with increasing oxidation time of more than 7.2 ks at 1473 K, and then after oxidation at 1573 K for 7.2 ks the particles disappeared. The scale surface on all the alloys was planar and the size of cavities on the scale surface of the standard, FZ, 0.5Pd, 0.5Pt, 0.05Y, 0.1Y, and 0.5Y alloys was 3, 2, 2, 2, 2, 1 and 1 μm, respectively, after oxidation at 1673 K for 18 ks.

$Y_3Al_5O_{12}$ particles were observed on the scale surface of the 0.1Y, 0.2Y and 0.5Y alloys after oxidation at 1673 K for 18 ks. The sizes of these particles were about 2 μm. The amounts of these particles increased with increasing yttrium content.

Acknowledgements

A part of this work was performed at Advanced Research Center of Metallic Glasses, Institute for Materials Research, Tohoku University. The authors are indebted to Mr. K. Obara of IMR, Tohoku University for helping to prepare the samples used in this study. This work was supported by the Grant-in-Aid for Scientific Research (No. 16560639), Japan.

References

[1] Y. Ikeda, K. Nii, C. Yoshihara, Trans. Japan Inst. Met. Suppl. (1983) 207.
[2] A.W. Funkenbusch, J.G. Smeggil, N.S. Bornstein, Met. Trans. 16A (1985) 1164.
[3] C. Mennicke, E. Schumann, J. Le Coze, J.L. Smialek, G.H. Meier, M. Rule, in: S.B. Newcomb, J.A. Little (Eds.), Microscopy of Oxidation, vol. 3, 1997, pp. 95–104.
[4] H. Al-Badairy, G.J. Tatlock, J. Le Coze, in: S.B. Newcomb, J.A. Little (Eds.), Microscopy of Oxidation, vol. 3, 1997, pp. 105–114.
[5] J.L. Smialek, in: S.B. Newcomb, J.A. Little (Eds.), Microscopy of Oxidation, vol. 3, 1997, pp. 127–139.
[6] P.Y. Hou, Z. Wang, K. Prusner, K.B. Alexander, I.G. Brown, in: S.B. Newcomb, J.A. Little (Eds.), Microscopy of Oxidation, vol. 3, 1997, pp. 140–149.
[7] P.Y. Hou, Oxid. Met. 52 (1999) 337.
[8] P.Y. Hou, J.L. Smialek, Mater. High Temp. 17 (2000) 79.
[9] T. Amano, T. Watanabe, K. Michiyama, J. Japan Inst. Met. 61 (1997) 1077.
[10] T. Amano, T. Watanabe, K. Michiyama, Oxid. Met. 53 (2000) 451.
[11] T. Amano, A. Hara, N. Sakai, K. Sasaki, Mater. High Temp. 17 (2000) 117.
[12] T. Amano, T. Watanabe, A. Hara, N. Sakai, H. Isobe, K. Sasaki, T. Shishido, ISIJ Int. 44 (2004) 145.
[13] T. Amano, S. Yajima, Y. Saito, Trans. Japan Inst. Met. Suppl. (1983) 247.
[14] H. Okabe, J. Japan Inst. Met. 49 (1985) 891.
[15] H. Okabe, J. Japan Inst. Met. 50 (1986) 500.
[16] T. Amano, K. Michiyama, K. Okazaki, In: L. Maldonado, M. Pech, (Eds.), Proceedings of 1st Mexican Symposium on Metal Corrosion, the Facultad de Quimica Press, Mexico, D.F. 1994, pp. 119–128, 258–264.
[17] A.S. Khanna, H. Jonas, W.J. Quadakkers, Werkstoffe Korrosion 40 (1989) 552.
[18] B.A. Pint, Oxid. Met. 45 (1996) 1.
[19] T. Amano, H. Isobe, N. Sakai, T. Shishido, J. Alloys Compd. 344 (2002) 394.
[20] K. Fukuda, K. Takao, T. Hoshi, Y. Usui, O. Furukimi, Mater. High Temp. 20 (2003) 319.
[21] S. Chevalier, J.P. Larpin, P. Dufour, G. Strehl, G. Borchardt, K. Przybylski, S. Weber, H. Scherrer, Mater. High Temp. 20 (2003) 365.
[22] B.A. Pint, K.L. More, I.G. Wright, Mater. High Temp. 20 (2003) 375.
[23] T. Amano, H. Isobe, K. Yamada, T. Shishido, Mater. High Temp. 20 (2003) 387.
[24] E.J. Felten, Oxid. Met. 10 (1976) 23.
[25] E.J. Felten, F.S. Pettit, Oxid. Met. 10 (1976) 189.
[26] I.M. Allam, H.C. Akuezue, D.P. Whittle, Oxid. Met. 14 (1980) 517.
[27] T. Amano, M. Okazaki, K. Takeuchi, T. Shishido, in: G.J. Tatlock, H.E. Evans (Eds.), Microscopy of Oxidation, vol. 6, 2005, pp. 309–316.
[28] V.K. Tolpygo, D.R. Clarke, Mater. High Temp. 17 (2000) 59.
[29] P.Y. Hou, A.P. Paulikas, B.W. Veal, in: G.J. Tatlock, H.E. Evans (Eds.), Microscopy of Oxidation, vol. 6, 2005, pp. 373–381.
[30] C.E. Holley Jr., F.B. Baker, in: L. Eyring (Ed.), Progress in the Science and Technology of Rare Earths, vol. 3, Pergamon Press, London, 1968, pp. 343–433.
[31] R. Prescott, M.J. Graham, Oxid. Met. 38 (1992) 233.
[32] C. Forest, H. Davidson, Oxid. Met. 43 (1995) 479.
[33] B.A. Pint, Oxid. Met. 48 (1997) 303.
[34] M.W. Brumm, H.J. Grabke, Corros. Sci. 33 (1992) 1677.
[35] R. Prescott, D.F. Mitchell, M.J. Graham, Corrosion 50 (1994) 62.
[36] V.K. Tolpygo, D.R. Clarke, Mater. High Temp. 20 (2003) 261.